NUMERICAL MODELING OF GENERALIZED NEWTONIAN FLOWS IN CHANNELS

Prokop, Vladimír
Department of Applied Mathematics, Faculty of Mechanical Engineering, Czech Teclmical University

Kozel, Karel
Department of Applied Mathematics, Faculty of Mechanical Engineering, Czech Teclmical University

出版情報：COE Lecture Note. 36, pp.63-72, 2012-01-27. 九州大学マス・フォア・インダストリ研究所
バージョン：
権利関係：

Proceedings of the Czech–Japanese Seminar in Applied Mathematics 2010
Czech Technical University in Prague, August 30 - September 4, 2010
pp. 63–72

NUMERICAL MODELING OF GENERALIZED NEWTONIAN FLOWS IN CHANNELS

VLADIMÍR PROKOP[1] AND KAREL KOZEL[1]

Abstract. This paper is concerned with numerical solution of generalized Newtonian flow in the channel geometry. This flow is described by the system of generalized Navier-Stokes equations. The system of equations consists of continuity and momentum equations. Viscosity in the momentum equations is not constant and is prescribed by a function depending on the shear rate. Numerical solution is based on the artificial compressibility method. Using this method allows us to solve hyperbolic-parabolic system of equations as a system of parabolic equations in time and to use time marching methods to find steady solution. Cell centered finite volume method is used for spatial discretization of the equations. Convective and viscous fluxes are computed using central discretization. Dual finite volume cells are used to compute spatial derivatives of the components of the velocity vector. Three-stage Runge-Kutta method is used for the solution of an arising system of ordinary differential equations. Unsteady computation is carried on by the dual-time stepping method.

Key words. generalized Newtonian fluid, Navier-Stokes equations, finite volume method, dual-time stepping method

AMS subject classifications. 76A05,76D05,76M12

1. Introduction. This paper deals with numerical solution of generalized Navier-Stokes equations in channel geometries. Solution of such a flow could be of interest in many industrial or biomedical applications. This work focuses mainly on the application of a simple mathematical model for blood flow. Blood is non-Newtonian suspension of blood cells in plasma. In some cases blood can be considered Newtonian, particularly in the vessels of big diameter, where the shear rate is high enough. Both, Newtonian and non-Newtonian cases of the flow are inspected in the geometry of the channel with bypass.

2. Mathematical model. The considered fluid (blood) is treated as an isothermal continuum. External forces are in this case neglected. The system of generalized Navier-Stokes equations is used to model incompressible viscous flow with variable viscosity. This system consists of equation of continuity and momentum equations [1] with variable viscosity:

$$\frac{\mathrm{d}\rho}{\mathrm{d}t} = 0 \quad \text{and therefore} \quad \vec{\nabla} \cdot \vec{w^*} = 0 \tag{2.1}$$

$$\rho \frac{\partial \vec{w^*}}{\partial t} + \rho \vec{\nabla} \cdot (\vec{w^*} \otimes \vec{w^*}) = \vec{\nabla} \cdot \boldsymbol{\sigma} \tag{2.2}$$

where ρ is density, $\vec{w^*} = (u^*, v^*)$ denotes velocity vector in 2D with physical components u^*, v^*. Cauchy stress tensor $\boldsymbol{\sigma}$ satisfies the following formula:

$$\boldsymbol{\sigma} = -p^* \mathbf{I} + 2\eta(\dot{\gamma})\mathbf{D} \tag{2.3}$$

[1]Department of Applied Mathematics, Faculty of Mechanical Engineering, Czech Technical University, Prague.

In the previous expression, p^* denotes physical pressure and $\mathbf{D} = \frac{1}{2}(\vec{\nabla}\vec{w}^* + (\vec{\nabla}\vec{w}^*)^T)$ in 2D is the symmetric part of velocity gradient (rate of deformation tensor), η is viscosity and $\dot{\gamma}$ is a shear rate. After regrouping and including the relation for $\boldsymbol{\sigma}$ and kinematic pressure $\bar{p} = p^*/\rho$, the equation (2.2) becomes

$$\frac{\partial \vec{w}^*}{\partial t} + \vec{\nabla} \cdot (\vec{w}^* \otimes \vec{w}^* + \bar{p}\mathbf{I}) = \frac{1}{\rho}\vec{\nabla} \cdot (2\eta(\dot{\gamma})\mathbf{D}) \tag{2.4}$$

The preceding equation (2.4) and eq. (2.1) rewritten in component form in 2D:

$$\frac{\partial u^*}{\partial x} + \frac{\partial v^*}{\partial y} = 0 \tag{2.5}$$

$$\begin{aligned} &\frac{\partial u^*}{\partial t} + \frac{\partial}{\partial x}((u^*)^2 + \bar{p}) + \frac{\partial}{\partial y}(u^* v^*) = \\ &= \frac{1}{\rho}\frac{\partial}{\partial x}\left(2\eta(\dot{\gamma})\frac{\partial u^*}{\partial x}\right) + \frac{1}{\rho}\frac{\partial}{\partial y}\left(\eta(\dot{\gamma})\left(\frac{\partial u^*}{\partial y} + \frac{\partial v^*}{\partial x}\right)\right) \end{aligned} \tag{2.6}$$

$$\begin{aligned} &\frac{\partial v^*}{\partial t} + \frac{\partial}{\partial x}(v^* u^*) + \frac{\partial}{\partial y}((v^*)^2 + \bar{p}) = \\ &= \frac{1}{\rho}\frac{\partial}{\partial x}\left(\eta(\dot{\gamma})\left(\frac{\partial v^*}{\partial x} + \frac{\partial u^*}{\partial y}\right)\right) + \frac{1}{\rho}\frac{\partial}{\partial y}\left(2\eta(\dot{\gamma})\frac{\partial v^*}{\partial y}\right) \end{aligned} \tag{2.7}$$

On the rigid boundary and at the inlet are prescribed Dirichlet boundary conditions for velocity and Neumann condition for pressure. At the outlet holds Neumann condition for velocity and Dirichlet condition for pressure.

2.1. Power-law model. The general constitutive equation for stress tensor for nonlinear viscous fluids is formulated as follows, see [4]:

$$\boldsymbol{\sigma} = -p^*\mathbf{I} + 2\eta(II_D, III_D)\mathbf{D} \tag{2.8}$$

where II_D, III_D are the second and third principal invariants of $\mathbf{D}$. Based on experimental results, see [4] the viscosity η depends only on the second invariant II_D:

$$II_D = -\frac{1}{2}\mathrm{tr}(\mathbf{D}^2) \tag{2.9}$$

where tr means trace. Shear rate or the metric rate of deformation is introduced and denoted by $\dot{\gamma}$:

$$\dot{\gamma} \equiv \sqrt{-4II_D} = \sqrt{2\mathrm{tr}(\mathbf{D}^2)} \tag{2.10}$$

The preceding equation (2.10) rewritten in the component form in 2D:

$$\dot{\gamma} = \sqrt{2\left(\frac{\partial u^*}{\partial x}\right)^2 + 2\left(\frac{\partial v^*}{\partial y}\right)^2 + \left(\frac{\partial u^*}{\partial y} + \frac{\partial v^*}{\partial x}\right)^2} \tag{2.11}$$

In this work only the power-law model is considered. In this case, viscosity η is given by the next formula:

$$\eta(\dot{\gamma}) = K\dot{\gamma}^{(n-1)}, \tag{2.12}$$

where K denotes consistency constant and n is the power-law index. This model is able to describe behavior of Newtonian and non-Newtonian shear-thinning and shear-thickening fluids depending upon the value of power-law index. The power-law index

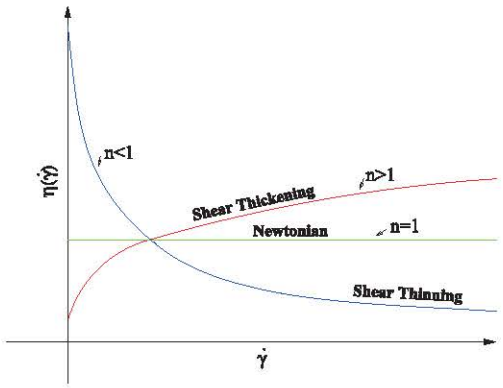

FIG. 2.1. *Viscosity as a function of shear rate for power-law fluids, a) shear-thinning ($n < 1$, b) constant viscosity ($n = 1$) ,c) shear-thickening ($n > 1$)*

$n = 1$ models Newtonian fluid with constant viscosity , $0 < n < 1$ describes shear-thinning fluid for which the viscosity decreases with increasing shear rate, $n > 1$ is used for shear-thickening fluid for which the viscosity increases as the fluid is subjected to higher shear rate. The figure 2.1 shows the dependence of viscosity η expressed by power-law model on the shear rate.

2.2. Generalized Navier-Stokes equations. The previous system of equations (2.6) – (2.7) is transformed into dimensionless vector form and the expression for viscosity η (2.12) is included:

$$\tilde{R}W_t + F^i_x + G^i_y = F^v_x + G^v_y, \qquad \tilde{R} = \mathrm{diag}\|0, 1, 1\| \tag{2.13}$$

where the subscripts $_{t,x\ ,y}$ denotes temporal and spatial derivatives. In the previous equation (2.13) $W = (p, u, v)^T$ is the vector of solution, $F^i = (u, u^2 + \tilde{p}, uv)^T$ and $G^i = (v, uv, v^2 + \tilde{p})^T$ are convective fluxes, $F^v = \frac{1}{Re}(0, 2\eta u_x, \eta(u_y + v_x))^T$ and $G^v = \frac{1}{Re}(0, \eta(v_x + u_y), 2\eta v_y)^T$ are viscous fluxes, $u = u^*/q_\infty, v = v^*/q_\infty$ are dimensionless components of the velocity vector and $p = p^*/\rho q^2_\infty$ is dimensionless pressure. Reynolds number in 2D for Newtonian fluid is given by the formula $Re = dq_\infty/\nu$, where q_∞ is the characteristic velocity (the speed of upstream flow), $\nu = \eta/\rho$ is the kinematic viscosity, d is the length scale (the width of the channel). The Reynolds number for non-Newtonian power-law fluid is expressed by $Re = \frac{\rho d^{(n)} q_\infty^{(2-n)}}{K}$.

3. Numerical solution. The system of generalized Navier-Stokes equations (2.13) is numerically solved by multistage Runge-Kutta method [5].

One approach to solve incompressible viscous flow is based on the idea to substitute time derivative of the pressure in the continuity equation. This is so called artificial compressibility method.

3.1. Artificial compressibility method. The artificial compressibility method is based on the addition of temporal pressure derivative divided by β^2 into the continuity equation, see [8]. The coefficient β is so called artificial speed of sound :

$$\frac{1}{\beta^2}\frac{\partial p}{\partial t} + \vec{\nabla} \cdot \vec{w^*} = 0, \quad \beta^2 \in \Re^+ \tag{3.1}$$

The boundary conditions are steady and the marching procedure converges to the steady state solution that does not depend on time and is also independent of the

parameter β. The choice of β is discussed in [9]. It is advised to choose β constant in the domain of the solution and the value of $\beta \approx \max_{V,s_i}(u_s)$, where V is domain of interest and s_i is the considered direction of space density of flux, u_s is the velocity in the direction s.

3.2. Finite volume method. The integral formulation of the conservation laws is discretized in space by means of the finite volume method (FVM) (see [7]). The domain Ω where the system of conservation laws is solved is divided into subdomains D_i. The sum of D_i covers the entire domain Ω and the following condition have to hold: $D_i \cap D_j = \emptyset$ for $i \neq j$

The finite volume method in cell-centered formulation is used. It means that pressure and two components of velocity are stored in the centers of finite volume cells.

Quadrilateral finite volumes are considered and the system of equations (2.13), where first equation is replaced with (3.1) so $\tilde{R} = \mathrm{diag}||1/\beta^2, 1, 1||$. This altered system of equations is multiplied by $\tilde{R}^{-1}$ and integrated over each finite volume cell. By the means of the mean value and Green's theorem one gets the system of ordinary differential equations:

$$W_t\,|_{i,j} = -\frac{1}{\mu_{i,j}} \sum_{k=1}^{4} (F^i - F^v)_{i,j,k} \Delta y_k - (G^i - G^v)_{i,j,k} \Delta x_k = -\mathrm{Rez} W_{i,j}, \tag{3.2}$$

where $F^i = (\beta^2 u, u^2 + \tilde{p}, uv)^T$ and $G^i = (\beta^2 v, uv, v^2 + \tilde{p})^T$ are convective fluxes and $F^v = \frac{1}{Re}(0, 2\eta u_x, \eta(u_y + v_x))^T$, $G^v = \frac{1}{Re}(0, \eta(v_x + u_y), 2\eta v_y)^T$ are viscous fluxes. Previous system of equations (3.2) with steady boundary conditions is solved using three-stage Runge-Kutta method that is of the second order of accuracy in time [3]:

$$W^n_{i,j} = W^{(0)}_{i,j} \tag{3.3}$$

$$W^{(r)}_{i,j} = W^{(0)}_{i,j} - \alpha_r \Delta t \overline{R} W^{(r-1)}_{i,j}, \quad r = 1, \ldots, 3 \tag{3.4}$$

$$W^{n+1}_{i,j} = W^{(m)}_{i,j}, m = 3, \tag{3.5}$$

$$\overline{R} W^{(r-1)}_{i,j} = \mathrm{Rez} W^{(r-1)}_{i,j} - D W^n_{i,j} \tag{3.6}$$

where $\alpha_1 = 0.5, \alpha_2 = 0.5, \alpha_3 = 1.0$. The term DW^n_{ij} is the term of artificial viscosity that is used to stabilize the computation [2]:

$$DW = D_x W + D_y W, \quad D_x W = d_{i+\frac{1}{2},j} - d_{i-\frac{1}{2},j}, \quad D_y W = d_{i,j+\frac{1}{2}} - d_{i,j-\frac{1}{2}} \tag{3.7}$$

$$d_{i+\frac{1}{2},j} = \frac{h_{i+\frac{1}{2},j}}{\Delta t} \epsilon^{(2)}_{i+\frac{1}{2},j} (W_{i+1,j} - W_{i,j}), \quad \nu^x_{i,j} = \frac{|p_{i+1,j} - 2p_{i,j} + p_{i-1,j}|}{|p_{i+1,j}| + 2|p_{i,j}| + |p_{i-1,j}|} \tag{3.8}$$

$$\epsilon^{(2)}_{i+\frac{1}{2},j} = \kappa^{(2)}_1 \max(\nu^x_{i+1,j}, \nu^x_{i,j}), \quad d_{i,j+\frac{1}{2}} = \frac{h_{i,j+\frac{1}{2}}}{\Delta t} \epsilon^{(2)}_{i,j+\frac{1}{2}} (W_{i,j+1} - W_{i,j}) \tag{3.9}$$

$$\nu^y_{i,j} = \frac{|p_{i,j+1} - 2p_{i,j} + p_{i,j-1}|}{|p_{i,j+1}| + 2|p_{i,j}| + |p_{i,j-1}|}, \quad \epsilon^{(2)}_{i,j+\frac{1}{2}} = \kappa^{(2)}_2 \max(\nu^y_{i,j+1}, \nu^y_{i,j}), \tag{3.10}$$

where $\kappa^{(2)}_{1,2}$ has to be chosen in order to achieve convergence of the method (in the computed cases were used values in the range $0.1 \to 0.5$), h denotes arithmetical average of the volumes of the cells adjacent to the face, where the value of d is computed, Δt is time step.

Formula for residual (2D) that appears in equation (3.6):

$$\mathrm{Rez}W_{ij} = \frac{1}{\mu_{ij}} \sum_{k=1}^{4} \left((F^i - F^v)_{ij,k} \Delta y_k - (G^i - G^v)_{ij,k} \Delta x_k \right) \tag{3.11}$$

Inviscid fluxes F^i are discretized centrally:

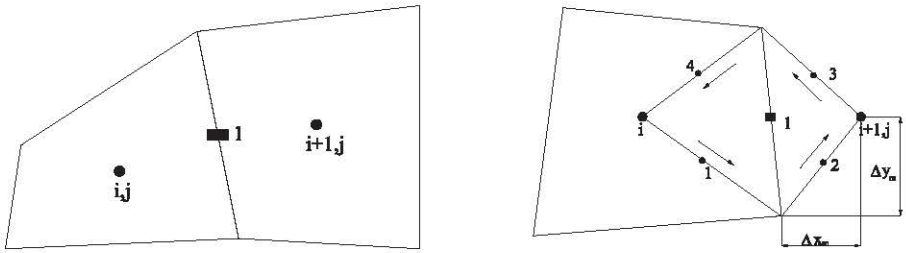

FIG. 3.1. **a)** *Approximation of the inviscid flux at the cell face* **b)** *Basic computational cell and dual cell for computation of velocity derivatives*

$$F^i_{i,j,1} = \frac{1}{2}(F^i_{i,j} + F^i_{i+1,j}) = \frac{1}{2}\left[\begin{pmatrix} \beta^2 u \\ u^2 + p \\ uv \end{pmatrix}_{i,j} + \begin{pmatrix} \beta^2 u \\ u^2 + p \\ uv \end{pmatrix}_{i+1,j} \right] \tag{3.12}$$

Discretization of viscous fluxes F^v is done by the means of dual volume cells:

$$F^v_{i,j,1} = \frac{1}{Re} \begin{pmatrix} 0 \\ 2\eta u_x \\ \eta(u_y + v_x) \end{pmatrix}_a, \quad G^v_{i,j,1} = \frac{1}{Re} \begin{pmatrix} 0 \\ \eta(v_x + u_y) \\ 2\eta v_y \end{pmatrix}_a \tag{3.13}$$

The following formulas describe numerical approximation of velocity derivatives in viscous fluxes, see fig. 3.2b:

$$u_x = \frac{1}{\mu_d} \oint_{\partial d} u dy \approx \frac{1}{\mu_d} \sum_{m=1}^{4} u_m \Delta y_m, \tag{3.14}$$

$$u_y = -\frac{1}{\mu_d} \oint_{\partial d} u dx \approx -\frac{1}{\mu_d} \sum_{m=1}^{4} u_m \Delta x_m, \tag{3.15}$$

where the velocity component u_m in the vertex of dual cell is either value of velocity in the center of basic cell or is computed as an average of four neighboring basic cells sharing considered vertex. The boundary of the dual cell is depicted by ∂d and μ_d is a volume of the dual cell.

3.3. Time step limitation. The considered Runge-Kutta scheme is explicit scheme and from its conditional stability one can obtain limitation on the time step. The system of Navier-Stokes or generalized Navier-Stokes equations, where convective and diffusive terms are discretized centrally, give rise to the following form of the time step limitation in two dimensions and for non-uniform, non-orthogonal grids, see [6]:

$$\Delta t = \min_{i,j} \frac{CFL|D_i|}{\rho_A \Delta y_{i,j} + \rho_B \Delta x_{i,j} + \frac{2\sqrt{\mathrm{tr}D^{2^T}}}{Re} \left(\frac{(\Delta x_{i,j})^2 + (\Delta y_{i,j})^2}{|D_i|} \right)}, \tag{3.16}$$

where $\rho_{\mathcal{A}} = |u| + \sqrt{u^2 + \beta^2}$ and $\rho_{\mathcal{B}} = |v| + \sqrt{v^2 + \beta^2}$ (when artificial compressibility method is used) are spectral radii of Jacobi matrices of convective fluxes $\mathcal{A} = \mathrm{d}F/\mathrm{d}W$ and $\mathcal{B} = \mathrm{d}G/\mathrm{d}W$, $|D_i|$ denotes the area of 2D finite volume cell, Δx_j and Δy_j are lengths of the j-th edges of the cell, CFL is Courante–Friedrich–Lewy number, and from von Neumann stability analysis for three stage Runge-Kutta method $CFL < 2$.

3.4. Implementation of boundary conditions.

Inlet: the extrapolation of the pressure is used and velocity profile is prescribed:

$$p_{in} = 2p_{in+1} - p_{in+2}, \quad u = u_\infty, v = 0, \tag{3.17}$$

where index $_{in}$ means position at the inlet cell, p is pressure, u, v are velocity components in the x, y directions and u_∞ describes inlet velocity profile.

Outlet: the extrapolation of the velocity vector, pressure has either given constant value or in the case of unsteady computation the value of the pressure is prescribed by some function:

$$u_{out} = 2u_{out-1} - u_{out-2},\ v_{out} = 2v_{out-1} - v_{out-2}, \tag{3.18}$$

$$p_{out} = p_{const}, \quad \text{or} \quad p_{out} = p_{const}(1 + \alpha \sin 2\pi\omega t), \tag{3.19}$$

where index $_{out}$ stands for the position at the outlet cell.

Wall: on the wall no-slip condition holds for viscous fluids and it is realized using ghost cells adjacent to the boundary:

$$u_{ghost} = -u_{inner},\ v_{ghost} = -v_{inner},\ w_{ghost} = -w_{inner},\ p_{ghost} = p_{inner}. \tag{3.20}$$

To fulfill no-slip condition the value of velocity components (depicted by an index $_{ghost}$) in the ghost cells have opposite signs to values in the inner cells adjacent to the boundary (depicted by an index $_{inner}$). Pressure p_{gjist} in the ghost cell has the same value as the pressure p_{inner} in the cell adjacent to the boundary.

3.5. Unsteady computation. The unsteady system of Navier-Stokes equations is solved either by the artificial compressibility method only or by the dual time stepping method.

In the artificial compressibility method for unsteady computation, the value of the artificial velocity of sound β must be now big positive number. The unsteady solution can be influenced by the addition of the term p/β^2 into the equation of continuity. This modified system of equation can be now directly solved by time-marching algorithm. The ideal value of β is when $\beta \to \infty$ but β also appears in the denominator of the formula that sets the value of the time step. Hence the value of β has to be limited from above in order to keep the value of the time step reasonably big for the numerical computation. The practical computations done in literature has shown that $\beta = 10$ is acceptable value.

The second possibility is the use of dual-time stepping method. To this end the system of Navier-Stokes equations (2.13) for unsteady flow is modified by addition of derivative of W in fictitious dual time, see [9]:

$$R_\beta W_\tau + RW_t + F_x^i + G_y^i = F_x^v + G_y^v \tag{3.21}$$

where the matrices R_β and R can be expressed as follows:

$$R_\beta = \begin{pmatrix} \frac{1}{\beta^2} & 0 & 0 \\ 0 & 1 & 0 \\ 0 & 0 & 1 \end{pmatrix} \quad R = \begin{pmatrix} 0 & 0 & 0 \\ 0 & 1 & 0 \\ 0 & 0 & 1 \end{pmatrix} \tag{3.22}$$

The artificial compressibility method is now applied on the fictitious dual time τ and next time level in the real time t is reached when the solution in dual time converges to the steady state. In this case $\beta \geq 1$ in order to $\frac{1}{\beta^2} \to 0$. To simplify the notation of the equation (3.21), the steady residual is introduced:

$$R_\beta W_\tau + RW_t + \mathrm{Res}^S(W) = 0, \tag{3.23}$$

where the steady residual is:

$$\mathrm{Res}^S(W) = (F^i - F^v)_x + (G^i - G^v)_y \tag{3.24}$$

The time derivative in the real time can be discretized by three–point backward formula and the unsteady residual can be written as follows:

$$\mathrm{Res}^U(W^{n+1}) = R\frac{3W^{n+1} - 4W^n + W^{n-1}}{2\Delta t} + \mathrm{Res}^S(W^{n+1}) \tag{3.25}$$

where index n denotes real time iteration and the scheme is implicit in the real time. The next equation can be solved by standard techniques for solution of steady flows (i.e. artificial compressibility method)

$$R_\beta W_\tau = -\mathrm{Res}^U(W^{n+1}) \tag{3.26}$$

The multistage Runge-Kutta method for the solution of the previous equation (3.26) can be written in the following form:

$$W_i^{(0)} = W_i^\nu \tag{3.27}$$

$$W_i^{(r+1)} = W_i^{(0)} - \alpha_r \Delta\tau \mathrm{Res}^U(W_i^{(r)}) \tag{3.28}$$

$$W_i^{\nu+1} = W_i^{(m+1)} \quad r = 0, \ldots, m \tag{3.29}$$

where the unsteady residual can be expressed:

$$\mathrm{Res}^U(W_i^\nu) = R\frac{3W^{n+1,\nu} - 4W^{n,\nu} + W^{n-1,\nu}}{2\Delta t} + \mathrm{Res}^S(W^{n+1,\nu}) \tag{3.30}$$

4. Results. In the first part of the result section numerical solution of Newtonian and non-Newtonian steady flow in the geometry of stenotic channel and bypass is presented as seen on the schematic figure 4.1. The upper part of the geometry of the channel is prescribed by the cosine function to simulate a stenosis with the following formula: $y = h{\cdot}\cos((2{\cdot}\pi{\cdot}(x_s - x_i)/x_l)))$, where the parameter $h = 0.35$ allows to change the height of the stenosis, $x_s = 3.7$ denotes the position where the stenosis starts, x_i describes actual position and x_l stands for the length of the part of the channel with stenosis. All these parameters can be changed in order to model different setups from mild to severe stenosis. The velocity profile at the inlet is computed in advance in a channel. The outlet pressure $p_{out} = 0.5$.

In the next series of figures 4.2,4.3,4.4, the simulation of Newtonian, shear-thinning and shear-thickening flow is presented for $Re = 200$ for geometry of the stenotic bypass and the channel. The channel is stenosed and the amount of the fluid volume is divided between the channel and the bypass as can be seen in the figure fig. 4.5 showing the velocity magnitude profiles in the cuts in the middle of the bypass and the channel. The velocity profile for shear-thinning fluid is sharper and for shear-thinning fluid flatter than in the case of Newtonian fluid. Prior to and behind

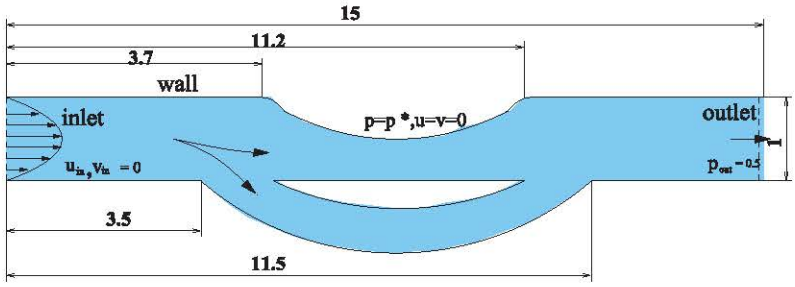

FIG. 4.1. *The geometry of the stenotic channel and the bypass*

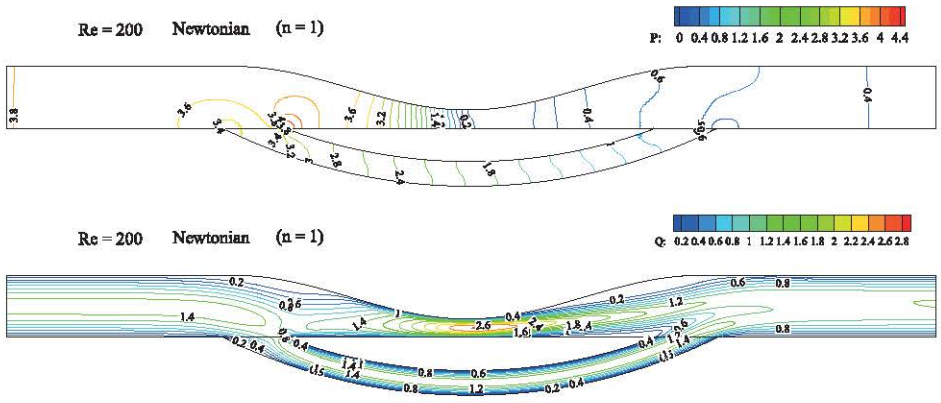

FIG. 4.2. *Stenotic channel and bypass, Re = 200, Newtonian steady flow, isolines of pressure and velocity magnitude*

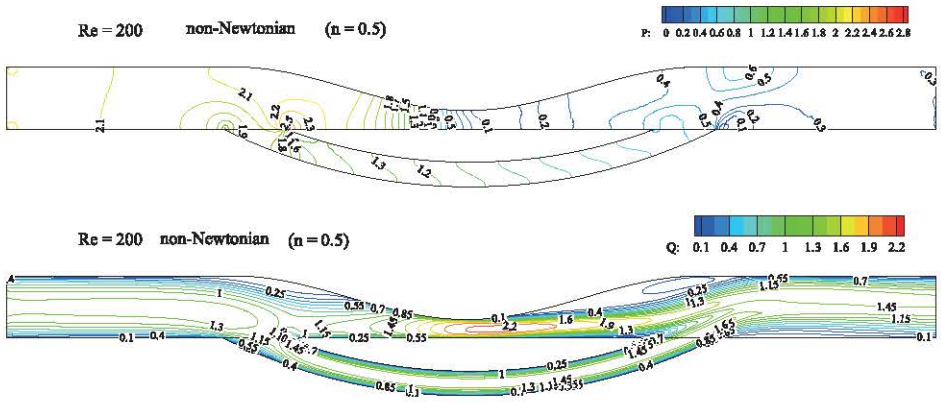

FIG. 4.3. *Stenotic channel and bypass, Re = 200, non-Newtonian steady flow, n = 0.5, isolines of pressure and velocity magnitude*

the stenosis strong zones of separation and reversal flow can be observed in the main channel.

In this section, the results of 2D unsteady simulation are presented in the stenotic channel with curved bypass. Firstly, the steady results for the chosen geometry must

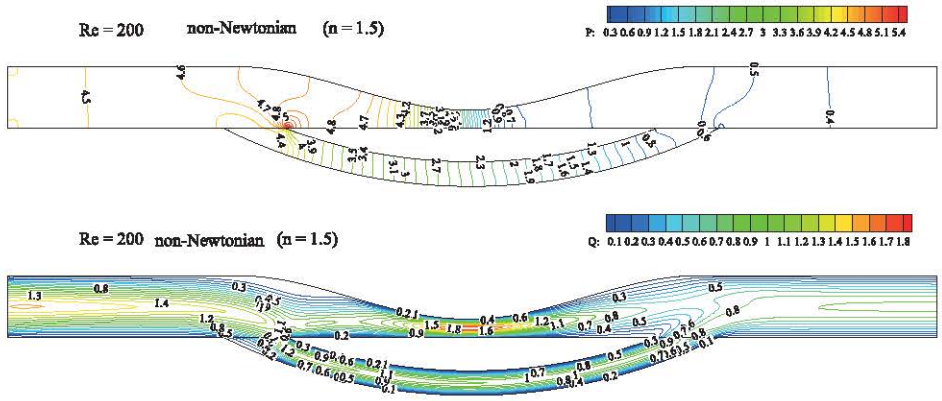

FIG. 4.4. *Stenotic channel and bypass, Re = 200, non-Newtonian steady flow, n = 1.5, isolines of pressure and velocity magnitude*

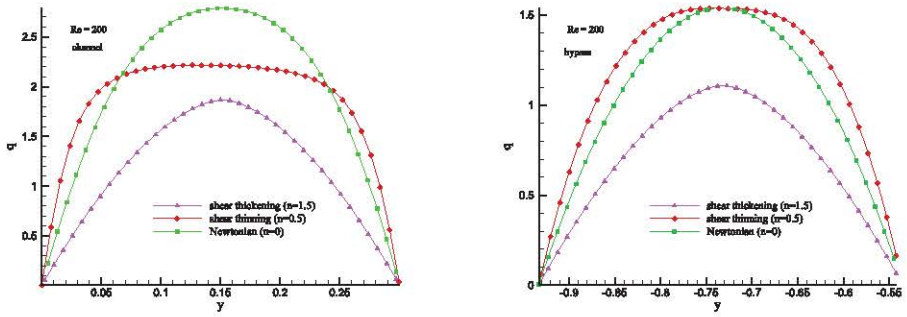

FIG. 4.5. *Stenotic channel and bypass, Re = 200, steady flow, comparison of velocity profiles in the middle of the channel and bypass*

be computed and then by the means of the artificial compressibility method the unsteady results are obtained. In this case the value of the parameter β in the artificial compressibility method, having meaning of the speed of sound, is set to $\beta = 10$ and the output pressure is prescribed with the following function: $p_2 = p_{20}(1 + \alpha \sin 2\pi\omega t)$, $\omega = 1Hz$, $p_{20} = 0.3$, $\alpha = 0.5$, where ω is a frequency and α is an amplitude. The pressure p_{20} is the same as the output pressure for the steady case. The series of figures fig.4.6 shows time evolution of unsteady non-Newtonian flow for $Re = 1000$ in one period with prescribed pressure oscillations at the outlet and $\beta^2 = 100$.

5. Conclusion. In this paper, the numerical model for Newtonian and non-Newtonian steady and unsteady laminar flows of incompressible viscous fluid was implemented. Numerical computations were performed in the geometry of the channel with bypass. Three values of power-law coefficient $n = 0.5$, $n = 1.0$, $n = 1.5$ representing shear-thinning, Newtonian and shear-thickening fluids were tested for different rather low Reynolds numbers from the range $< 200; 1000 >$. Unsteady computations were done in the same geometries for frequency $f = 1Hz$.

The achieved results are useful in the numerical simulation of blood flow in the

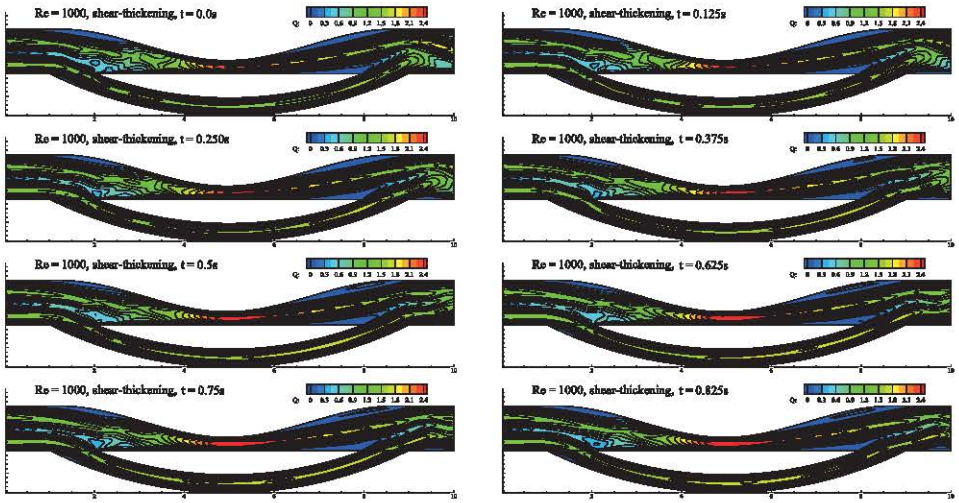

FIG. 4.6. *Unsteady non-Newtonian flow in bypass, Re=1000,* $n = 1.5$, $p_2 = p_{20}(1 + \alpha \sin 2\pi f t)$, $f = 1Hz, p_{20} = 0.3, \alpha = 0.5$, *isolines of velocity magnitude*

geometry of vessel and bypass after further improvements would be done.

Acknowledgment. This work was sponsored by Research Plan MSM 6840770010, GA ASCR No. IAA 100190804, GA CR No. 101/09/1539

REFERENCES

[1] M. BRDIČKA ET AL. *Continuum Mechanics.* Academia, Prague (2000).
[2] A. JAMESON, W. SCHMIDT AND E. TURKEL. *Numerical solution of the Euler equations by finite volume methods using Runge-Kutta time-stepping schemes.* AIAA (1981), 1981-1259.
[3] CH. HIRSCH. *Numerical Computation of Internal and External Flows.* Butterworth-Heinemann, 2nd edition (2007).
[4] G. P. GALDI, R. RANNACHER, A. M. ROBERTSON AND S. TUREK. *Hemodynamical flows, modeling, analysis and simulation*, Birkhauser Verlag AG, Basel, (2008).
[5] J. BLAZEK. *Computational Fluid Dynamics: Principles and Applications.* Elsevier, Amsterdam (2001).
[6] R. KESLEROVÁ AND K. KOZEL. *Numerical solution of 2D and 3D incompressible laminar flows through a branching channel.* In: Proc. Topical problems of fluid mechanics, Prague, 2005, 55–58.
[7] R. J. LEVEQUE. *Numerical methods for conservation laws.* Birkhauser Verlag, Basel (1990).
[8] A. J. CHORIN. *A Numerical method for solving incompressible viscous flow problems.* Journal of Computational Physics **135** (1997), 118–125.
[9] J. FOŘT, K. KOZEL, P. LOUDA AND J. FÜRST. *Numerical methods solving the flow problems III.* (In Czech), CTU Prague (2004).
[10] A. SEQUEIRA AND J. JANELA. *An overview of some mathematical models of blood rheology.* In: M. S. Pereira (ed.), A portrait of state-of-the-art research at the Technical University of Lisbon, 65–87, Springer (2007).